EARTH SURFACE PROCESSES AND LANDFORMS
Earth Surf. Process. Landforms **45**, 3842–3853 (2020)

Published online 1 October 2020 in Wiley Online Library
(wileyonlinelibrary.com) DOI: 10.1002/esp.5004

Holocene climate forcings and lacustrine regime shifts in the Indian summer monsoon realm

Sushma Prasad,[1,3]* Norbert Marwan,[2,3] Deniz Eroglu,[4] Bedartha Goswami,[2] Praveen K. Mishra,[5] Birgit Gaye,[6] A. Anoop,[7] N. Basavaiah,[8] Martina Stebich[9] and Arshid Jehangir[10]

[1] ERA Scientific Editing, Grosse Fischerstrasse 10, Potsdam D-14467, Germany
[2] Potsdam Institute for Climate Impact Research (PIK), Member of the Leibniz Association, P.O. Box 60 12 03, Potsdam D-14412, Germany
[3] Institute for Earth Science, University of Potsdam, Karl-Liebknecht-Straße 24-25, Potsdam D-14476, Germany
[4] Department of Bioinformatics and Genetics, Kadir Has University, Istanbul 34083, Turkey
[5] Wadia Institute of Himalayan Geology, 33 GMS Road, Dehradun 248001, India
[6] Universität Hamburg, Institute for Geology, Hamburg, Germany
[7] Department of Earth and Environmental Sciences, Indian Institute of Science Education and Research (IISER) Mohali, Sector 81, SAS Nagar, Manauli, Punjab 140306, India
[8] Indian Institute of Geomagnetism, New Panvel, Mumbai, Maharashtra 410206, India
[9] Senckenberg Research Institute, Research Station of Quaternary Palaeontology, Am Jakobskirchhof 4, Weimar D-99423, Germany
[10] Department of Environmental Science, University of Kashmir, Srinagar, Jammu & Kashmir 190006, India

Received 20 May 2019; Revised 29 August 2020; Accepted 31 August 2020

*Correspondence to: Sushma Prasad, ERA Scientific Editing, Grosse Fischerstrasse 10, 14467 Potsdam, Germany. E-mail: sprasad@erascientificediting.com

ESPL
Earth Surface Processes and Landforms

ABSTRACT: Extreme climate events have been identified both in meteorological and long-term proxy records from the Indian summer monsoon (ISM) realm. However, the potential of palaeoclimate data for understanding mechanisms triggering climate extremes over long time scales has not been fully exploited. A distinction between proxies indicating climate change, environment, and ecosystem shift is crucial for enabling a comparison with forcing mechanisms (e.g. El-Niño Southern Oscillation). In this study we decouple these factors using data analysis techniques [multiplex recurrence network (MRN) and principal component analyses (PCA)] on multiproxy data from two lakes located in different climate regions – Lonar Lake (ISM dominated) and the high-altitude Tso Moriri Lake (ISM and westerlies influenced). Our results indicate that (i) MRN analysis, an indicator of changing environmental conditions, is associated with droughts in regions with a single climate driver but provides ambiguous results in regions with multiple climate/environmental drivers; (ii) the lacustrine ecosystem was 'less sensitive' to forcings during the early Holocene wetter periods; (iii) archives in climate zones with a single climate driver were most sensitive to regime shifts; (iv) data analyses are successful in identifying the timing of onset of climate change, and distinguishing between extrinsic and intrinsic (lacustrine) regime shifts by comparison with forcing mechanisms. Our results enable development of conceptual models to explain links between forcings and regional climate change that can be tested in climate models to provide an improved understanding of the ISM dynamics and their impact on ecosystems. © 2020 John Wiley & Sons, Ltd.

Introduction

The Indian summer monsoon (ISM) provides 80% of the total annual rainfall and governs the livelihood of millions of people on the Indian subcontinent (Sahai *et al.*, 2003; Goswami *et al.*, 2006; Prasanna, 2014). Though its long-term trend has been linked to changes in solar insolation (Fleitmann *et al.*, 2003; Gupta *et al.*, 2005; An *et al.*, 2012; Sarkar *et al.*, 2015; Mishra *et al.*, 2018a), both modern (Goswami *et al.*, 2006) and palaeo-ISM (Sinha *et al.*, 2011; Dixit *et al.*, 2014a, Dixit *et al.*, 2014b; Raj *et al.*, 2015; Bhushan *et al.*, 2018) are punctuated by extreme climate events that have been attributed to the effect of ocean–atmosphere teleconnections [e.g. ENSO (El-Niño Southern Oscillation)] (Prasad *et al.*, 2014) or northern hemisphere cooling (Menzel *et al.*, 2014). The non-stationary nature of such forcings (Kumar *et al.*, 1999; Prasad *et al.*, 2014) precludes a simplistic predictive modelling of the ISM (Gadgil *et al.*, 2004; Bird *et al.*, 2014; Chen *et al.*, 2019). Presently, the future evolution of the ISM under greenhouse warming conditions is uncertain, with different modelling scenarios ranging from slight to no increase in extremes (Shashikanth *et al.*, 2018), to an intensification of extreme events with no change in annual rainfall (Goswami *et al.*, 2006), or even a stronger ISM (Wang *et al.*, 2013). Given the wide range of future ISM scenarios, and their role in global climate, it is crucial to identify forcings that might result in amplified monsoon variability and trigger ecological regime shifts. We adhere to the following definition: 'a regime shift occurs when an internal feedback or an external forcing triggers a different system behaviour' (Scheffer *et al.*, 2001; Folke *et al.*, 2004). The regime shifts may be extrinsic (driven by externally forced climate change, e.g. by insolation, ENSO)

or intrinsic (resulting from thresholds or nonlinear responses of ecosystems to climate change) (Eroglu *et al.*, 2016). It is potentially possible to distinguish between the two types of regime shifts by comparing proxy records with known forcings.

Data analyses allow us to track temporal coherence between climate proxies and forcings, enabling an understanding of the underlying system dynamics. To date, these techniques have largely been applied to high-resolution ice core and stalagmite data (Williams *et al.*, 2011; Thomas, 2016; Lechleitner *et al.*, 2017). These archives have neither widespread geographical coverage, nor do they provide insights into ecological regime shifts. Techniques, including those based on recurrence methods, for data with age uncertainties or irregular sampling (Rehfeld *et al.*, 2011; Eroglu *et al.*, 2016; Goswami *et al.*, 2018) must be tested on other widespread multiproxy archives (e.g. lakes) to obtain insights into climate forcings that trigger extreme events and cause long-term ecological regime shifts. Analysis of multiproxy palaeodata can additionally provide information on regional differences in the sensitivity of different components of the ecosystem to climate forcings. However, this approach is not free from challenges. In a multiproxy approach to palaeoclimate reconstruction, an apparent proxy response may be dependent upon additional factors such as sample location within the studied archive, provenance change, or human influence (Lotter, 2003; Birks and Birks, 2006). A palaeoclimate reconstruction based on a limited number of proxies raises the question of whether the so-called 'climate shift' actually represents a 'regime shift'. A multiproxy record offers the potential to distinguish the two, and thereby document the impact of climate change on the ecosystem. For example, an evaporite layer might indicate the terminal phase of a drying event which might have begun decades/centuries earlier and was preserved in geochemical/biological proxies. In this case, the former might represent a regime shift rather than a climate change that began significantly earlier. The distinction between the two is necessary to recognize the timing of climate change and identify its impact on the ecosystem. This, in turn, will enable the comparison of independently derived palaeorecords with known forcing mechanisms, and the development of hypotheses that can be tested against climate model simulations.

The prerequisites for our study are (i) a comprehensive database on catchment and modern lacustrine sediments that clearly characterizes proxy links to catchment change, climate, and environmental conditions; (ii) availability of the same proxies in well-dated cores; (iii) archives from at least two different climate regions to test the applicability of data analysis techniques and identify overarching climate forcing mechanisms.

In this study we aim to test two different methods: (a) multiplex recurrence network (MRN) to identify lacustrine regime changes on the basis of similarity in behaviour of proxies in response to a strong environmental forcing; (b) principal component analysis (PCA) to characterize the response of different proxies to climate and (external/internal) lacustrine regime shifts. We focus on 8.4 ka of palaeoclimate data from two lakes located in different climate regions: the central Indian Lonar Lake from the core ISM zone (Gadgil, 2003) and the Tso Moriri Lake located in the high-altitude desert of the NW Himalaya which is influenced by the winter westerlies and peripherally by the ISM. Modern sediments from both the lakes have been investigated extensively for establishing proxy–climate linkages (Menzel *et al.*, 2013; Basavaiah *et al.*, 2014; Mishra *et al.*, 2014; Riedel *et al.*, 2015). We aim to (i) identify changes in proxy dynamical behaviour and their association with extreme climate events; (ii) detect links between specific proxies and climate processes (evaporation, precipitation) in different climate regions; (iii) differentiate between externally and internally forced regime shifts; (iv) assess regional differences in the impact of known climate forcings against the background of changes in solar insolation and northern hemisphere cooling; and (v) identify intervals when regimes shifts were frequent.

Study Area and Chronology

Lonar Lake

Lonar Lake, a meteorite impact crater (Jourdan *et al.*, 2011) in the Deccan flood basalts (Figures 1a and b), lies in the Buldhana district of Maharashtra State, India (19°58′N, 76°30′E; 600 m a.s.l.). The closed (endorrheic) lake is hyposaline and alkaline (pH varies between 9.5 and 10.4) (Jhingran and Rao, 1958; Joshi *et al.*, 2008) with an anoxic bottom layer below 4 m water depth (AD 2011) (Basavaiah *et al.*, 2014). It is fed by surface runoff from ISM precipitation and three perennial streams. Since the lake has no outlet, water level is controlled by the balance between evapotranspiration and precipitation, with minor contribution from groundwater-fed springs. Modern-day summer rainfall (c. 680 mm, Figure 1d) in the Lonar region is largely provided by the Arabian Sea branch of the southwest monsoon (Sengupta and Sarkar, 2006; Mishra *et al.*, 2018b). The water level in the Lonar Lake fluctuates in response to ISM precipitation, with higher lake level during stronger monsoon years (Anoop *et al.*, 2013a). The modern vegetation in the Lonar region represents a tree savanna with an open woody cover and continuous C4 grass undergrowth (Riedel *et al.*, 2015).

The chronology (Figure 3a) of the Lonar Lake core sediments is based on 18 ^{14}C dates obtained from wood, leaf, bulk organic material, and gaylussite crystals (Anoop *et al.*, 2013a; Prasad *et al.*, 2014) that were calibrated using OxCal 4.1 software (Ramsey, 2008, 2009) with the IntCal09 calibration curve (Reimer *et al.*, 2009).

Tso Moriri Lake

Tso Moriri Lake (Figures 1a and c) is a brackish water body situated in a high-altitude desert (32°40′–33°02′N, 78°14′–78°25′E; ~4600 m a.s.l.) in NW Himalaya (Leipe *et al.*, 2014; Mishra *et al.*, 2014, 2015). The lake has a length of c. 22 km (in N–S direction), with an average width of 5 km and a surface area of ~150 km^2 (Mishra *et al.*, 2014). The maximum water depth in the lake is 105 m. The hydrology of the Tso Moriri Lake is governed by the interplay between precipitation (ISM and westerlies), snowmelt, and evaporation (Mishra *et al.*, 2015). Along with several ephemeral streams, the lake is fed by meltwater from two major streams: Gyoma (from the north) and Phirse Phu (from the south). The Tso Moriri region receives 70% of precipitation (Figure 1d) in the form of snow during October to April, with peripheral ISM influence (Leipe *et al.*, 2014). The mean temperature in the region varies between 0 to 30 °C (during summer) and −40 to −10 °C (during winter) (Mishra and Humbert-Droz, 1998). The high-altitude lake is surrounded by sparse desert-steppe vegetation.

The chronology (Figure 3b) of the Tso Moriri sediment core is based on ^{14}C AMS dates of seven bulk sediments, five organic fragments of macrophyte (*Potamegeton pectinatus*), and a terrestrial twig (Mishra *et al.*, 2015). ^{14}C dates on a modern sample of macrophyte and bulk sediment (0–1 cm) were used to correct for the hard-water effect in the core sediments. An online version of OxCal 4.2 software and IntCal13 calibration curve were used to calibrate the radiocarbon ages (Reimer *et al.*, 2009).

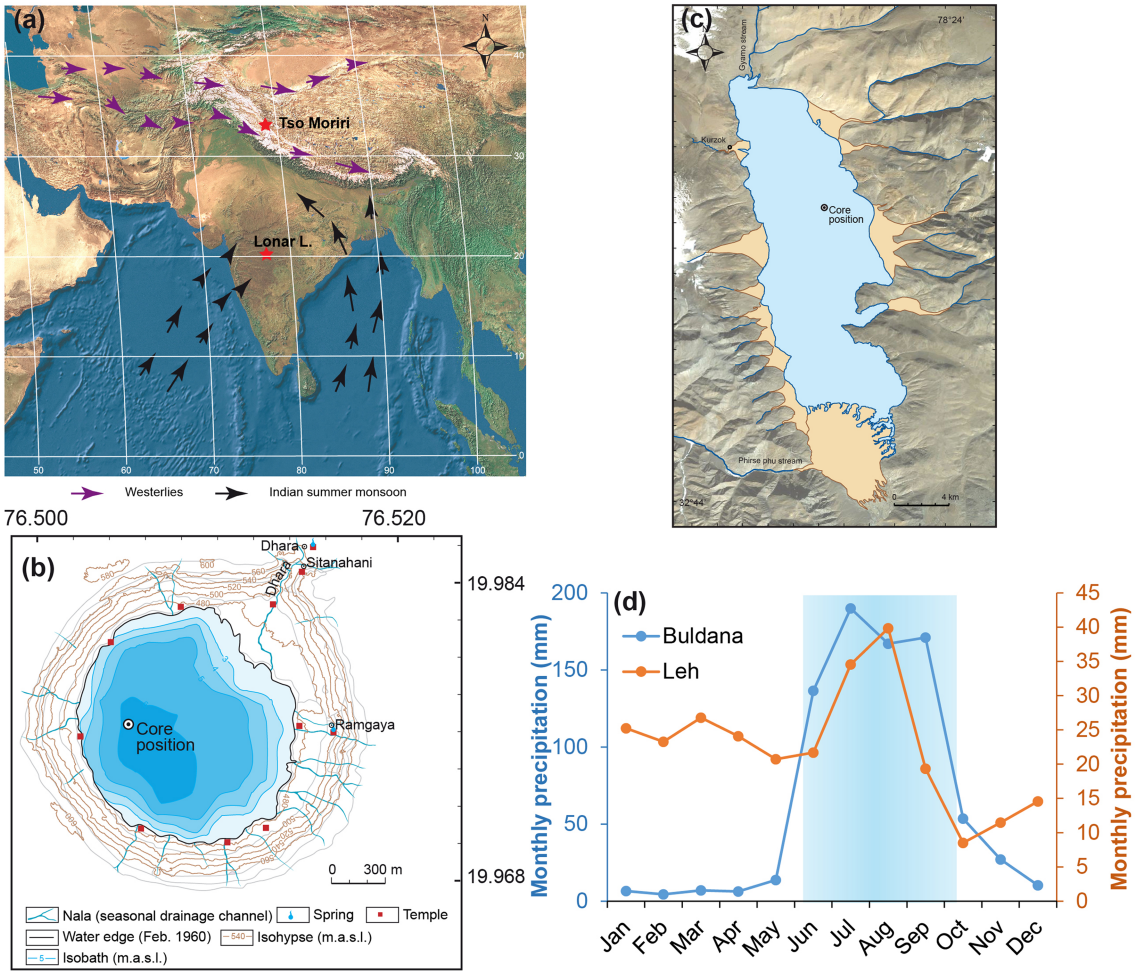

Figure 1. (a) Precipitation pathways in the ISM realm and the location of Lonar and Tso Moriri lakes. Black (purple) arrows represent ISM (westerlies); (b, c) show location of long cores. Average monthly precipitation in locations closest to Lonar (Buldana) and Tso Moriri (Leh) is shown in (d). [Colour figure can be viewed at wileyonlinelibrary.com]

Climate significance of investigated proxies

An in-depth understanding of the environmental sensitivity of proxies is essential for interpreting the results of the performed statistical analyses (MRN and PCA). Detailed results on proxy significance have been published in Basavaiah *et al.* (2014), Prasad *et al.* (2014), Mishra *et al.* (2014, 2015), and a summary is presented here. The lithogenic input reflects the precipitation amount and inflow energy, the catchment geology, and is also related to vegetation cover (Mishra *et al.*, 2015). Changes in lithogenic distribution within the lake are indicative of hydrodynamic conditions during the sedimentation process (Mishra *et al.*, 2014). Investigations on modern lake surface sediments indicate that in a large lake system like the Tso Moriri an increase (decrease) in lithogenic contribution reflects higher (lower) inflow into the lake (Mishra *et al.*, 2014). However, in shallow lake systems like the Lonar, higher (lower) lithogenic content is an indicator of lower (higher) lake level and shoreline proximity (Basavaiah *et al.*, 2014). The total organic carbon (TOC) and total nitrogen (TN) deposited in the sediments was derived from a combination of terrestrial and aquatic sources. The C/N ratio is often used to decipher past changes in primary lacustrine productivity (Anoop *et al.*, 2013a). The aquatic organisms (e.g. phytoplankton and zooplankton) are rich in protein, but have less cellulose content, and are characterized by low C/N ratios (4 to 10) (Meyers, 1997; Prasad *et al.*, 2016). However, the lignin-rich terrestrial plants are characterized by higher C/N ratios (≥20) (e.g. Prasad *et al.*, 1997; Xu *et al.*, 2006). In both lakes the organic matter contains a mixture of terrestrial and aquatic vegetation (Menzel *et al.*, 2013; Basavaiah *et al.*, 2014; Mishra *et al.*, 2014; Prasad *et al.*, 2014; Sarkar *et al.*, 2015). Changes in phytoplankton biological productivity can be inferred from variations in carbon and nitrogen isotopes of bulk organic matter. $\delta^{13}C$ values of terrestrial organic material are mainly determined by the contribution of plants using the C3 (wetter conditions; $\delta^{13}C = -25$ to $-30‰$) or the C4 (drier conditions; $\delta^{13}C = -10$ to $-15‰$) pathway for CO_2 uptake by plants (Meyers and Ishiwatari, 1993). The $\delta^{13}C$ record is also governed by changes in organic productivity, salinity, and pH of the water (Stuiver, 1975). Photosynthetic productivity preferentially uses ^{12}C and ^{14}N, leaving the DIC and DIN pools enriched in ^{13}C and ^{15}N, respectively (Swart, 1983; Talbot and Lærdal, 2000); hence intervals of increased productivity are marked by increased $\delta^{13}C$ and $\delta^{15}N$ values of phytoplankton (Hodell and Schelske, 1998). Stronger evaporation during drier conditions results in alkaline conditions, relatively higher phytoplankton productivity, and enhanced $\delta^{13}C$ and $\delta^{15}N$ (Menzel *et al.*, 2013; Basavaiah *et al.*, 2014). The isotopic composition of endogenic carbonate minerals precipitated during summer evaporation is used as a proxy to ascertain the extent of evaporation, and precipitation pathways (Anoop *et al.*, 2013a; Mishra *et al.*, 2014, 2015).

Holocene climate variability at investigated sites

The multiproxy data from Lonar Lake (Figure 2a) showed solar insolation-driven early Holocene ISM intensification (Prasad

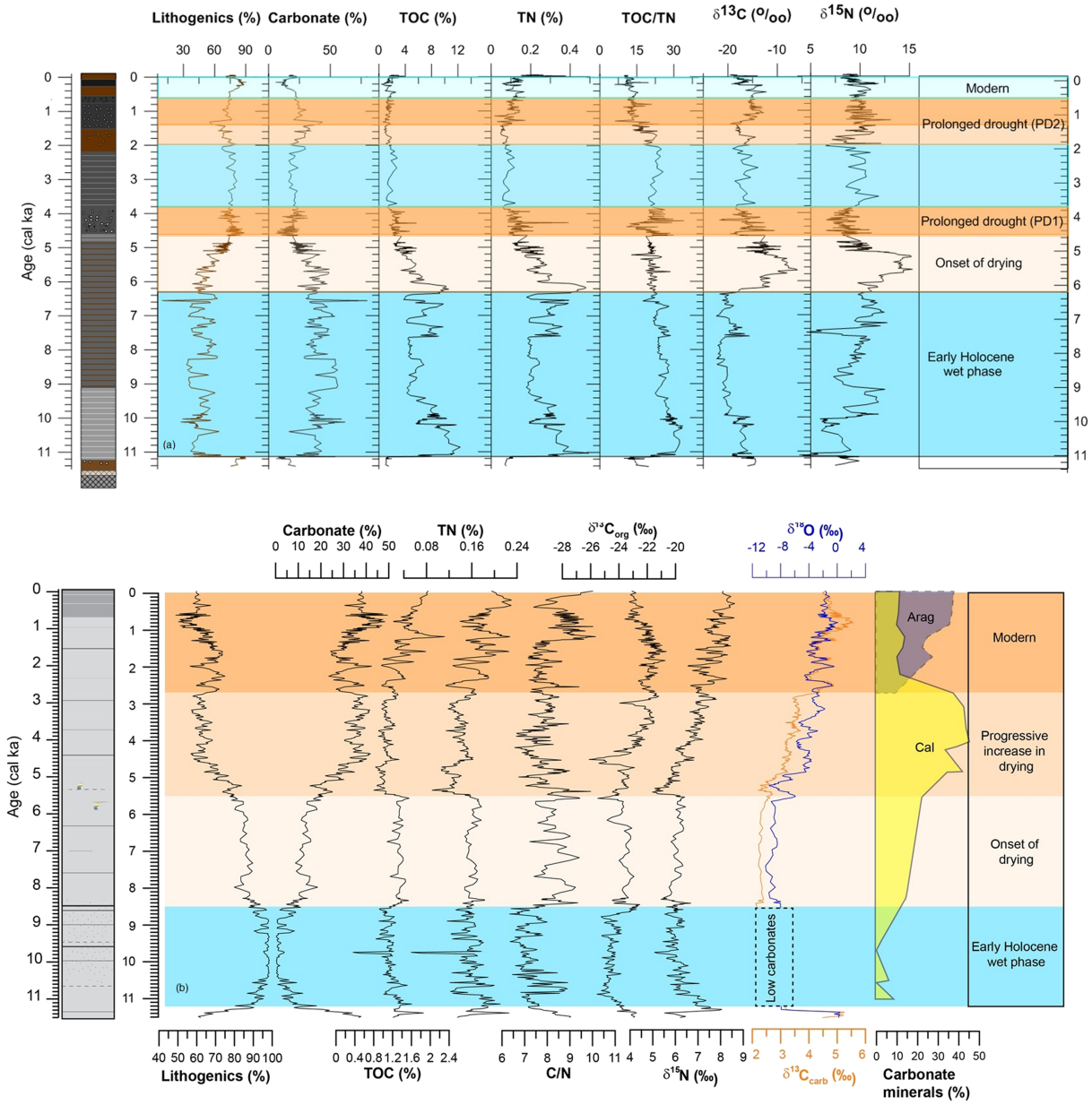

Figure 2. (a) Litholog, multiproxy data, and reconstructed palaeoclimate from the central Indian Lonar (a) and Tso Moriri lakes (b). Horizontal lines in the lithologs indicate lamination. The white dots in the Lonar litholog (a) represent gaylussite crystals formed during prolonged droughts. Blue (brown) bars in both lithologs indicate wet (dry) periods, respectively, with darker shading indicating intensity. [Colour figure can be viewed at wileyonlinelibrary.com]

et al., 2014). The ISM weakening beginning c. 6.2 cal ka was nonlinear with two prolonged droughts (PD, centennial periods of weaker monsoon) between 4.6–3.9 (PD1) and 2–0.6 cal ka (PD2), which were identified by the presence of the evaporite mineral gaylussite (Anoop *et al.*, 2013a) (Figure 2a). The so-called global 'events' (4.2 ka and the 8.2 ka events) were not very clearly evidenced in the geochemical or bulk organic isotopic data (Menzel *et al.*, 2014). Human influence on the lake system from 1.2 cal ka is evident, based on organic proxies (C/N, $\delta^{13}C_{org}$) and the pollen assemblage (Mishra *et al.*, 2018b). The pollen record of Lonar Lake indicates the existence of moist to wet semi-evergreen forest during the early to mid-Holocene, featuring a C3 grass undergrowth. Biomarker isotope data indicates gradual establishment of C4 grasses with increasing aridity (Sarkar *et al.*, 2015). A change in vegetation type is indicated in the pollen record by a rapid decrease of evergreen woody elements at 5.0 cal ka, with an increase in dry deciduous and xeric trees and shrubs. The spread of thornshrub-savanna reflects enhanced aridity between 4 and 3.5 cal ka. Stronger monsoon activity is indicated by an increased share of dry deciduous forest elements between 3.5 and 2.0 cal ka with an accompanying decrease in taxa of xeric woodland (including thornshrubs). Thereafter, xeric thornshrubs increase again following a second prolonged shift to more arid conditions.

Regional W–E palaeohydrological transects indicate that the lake-level changes in Tso Moriri since the early Holocene preserve the record of interplay between ISM and mid-latitude westerlies (Mishra *et al.*, 2018a). The mineralogy and isotopic composition of endogenic carbonates (calcite and aragonite), and geochemical data from the Tso Moriri Lake sediments (Figure 2b), have been utilized to understand the hydrological changes during the Holocene (Mishra *et al.*, 2015). The low percentages of endogenic carbonates, and depleted $\delta^{18}O$ between 11.2 and 8.5 cal ka, suggest freshwater conditions and highest lake level (an abrupt increase of c. 47 m; Mishra *et al.*, 2018a) resulting from increased ISM precipitation and reduced evaporation. The progressive enrichment in $\delta^{18}O$ and reappearance of endogenic carbonates between 8.5 and 5.5 cal ka (Figure 2b) indicate a weakening of ISM with decreasing solar insolation and increased westerlies. The

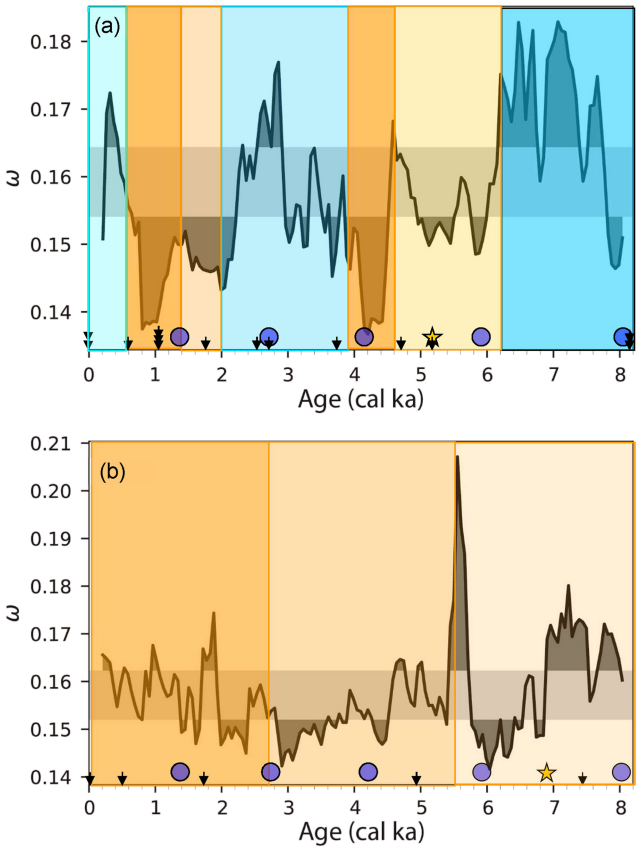

Figure 3. Illustration of derived average edge measure calculated in moving windows for Lonar (a) and Tso Moriri (b) multiproxy data. The shaded grey area marks the upper 95% confidence interval. The brown vertical bars indicate prolonged drier periods identified by mineralogical changes – darker colours indicate intensity. The solid blue circles along the age axis indicate peak events in the discharge of IRD in the north Atlantic (Bond *et al.*, 1997). All IRD events coincide with intervals of less dynamical behaviour (i.e. drier events). Yellow stars indicate additional drier events. Downward-facing arrows on the age axis indicate radiocarbon dates. [Colour figure can be viewed at wileyonlinelibrary.com]

period between 5.5 and 2.7 cal ka was characterized by a weaker monsoon, increasing dryness, and lowering of the lake level. This was followed by intensified drying (precipitation of aragonite), resulting in the onset of modern-day conditions after c. 2.7 cal ka (Mishra *et al.*, 2015). The Tso Moriri pollen record suggests that alpine steppe vegetation was dominant throughout the entire Holocene, with an admixture of alpine tundra and desert elements (Leipe *et al.*, 2014). Pollen-based moisture reconstruction indicates an overall trend towards drier conditions during the past 10 cal ka, paralleling the reduction in the Northern Hemisphere summer insolation.

Methods

To investigate the temporal stability of the proxies, we have applied techniques that quantify the simultaneous variability of selected proxies representing erosion/inflow (lithogenics), evaporative (carbonate %, $\delta^{13}C_{carb}$, $\delta^{18}O_{carb}$), and biological processes [TOC (%), C/N, $\delta^{13}C_{org}$, $\delta^{15}N_{org}$] within the lake. Although additional proxies (mineralogy, biomarkers, amino acids) are available, they have been excluded from data analyses because of their low temporal resolution. As seen in Figures 2a and b, not all proxies are continuously available throughout the Holocene. Hence, investigations in both lakes are limited to 8.4 cal ka.

Multiplex recurrence network

This method constructs an m-layer network from m time series (Eroglu *et al.*, 2018). Each layer of an MRN consists of a recurrence network (RN) (Marwan *et al.*, 2009) where the layers are connected to each other with the same time-labelled nodes. An RN is a binary square matrix **A** where the columns and rows represent time and entry one represents a time pair when the same state appeared at these time points (recurrence), an entry with zero which mean that there are different states at these times. In contrast to standard time-series analysis techniques, an MRN considers and evaluates the synchronous variability of several proxy records at the same time; however, the values of the proxies can still differ significantly. By applying a moving-window approach, entrapped climate transitions in data can be identified.

From an m-dimensional multivariate time series (with length N), we have constructed a large adjacency matrix describing the entire multiplex network denoted by

$$\mathbf{A} = \begin{bmatrix} A^{[1]} & \mathbf{I}_N & \cdots & \mathbf{I}_N \\ \mathbf{I}_N & A^{[3]} & \ddots & \vdots \\ \vdots & \ddots & \ddots & \mathbf{I}_N \\ \mathbf{I}_N & \cdots & \mathbf{I}_N & A^{[m]} \end{bmatrix}$$

where $\mathbf{I}_N$ is the identity matrix of size N. We denote the adjacency matrix of the RN at the κ^{th} layer as $A^{[\kappa]} = a_{ij}^{[\kappa]}$ and $a_{ij}^{\kappa} = 1$ if nodes i and j are connected in layer κ, $a_{ij}^{\kappa} = 0$ otherwise. A connection of nodes i and j corresponds to a recurrence of the states at times i and j (i.e. the states at i and j are very similar). In order to quantify the coherence (the synchronous dynamical variability) of the original multivariate system by the MRN, we use the *average edge overlap*

$$\omega = \frac{\sum_i \sum_{j>i} \sum_K a_{ij}^{[K]}}{m \sum_i \sum_{j>i} \left(1 - \delta_{0, \sum_K a_{ij}^{[K]}}\right)}$$

where δ_{ij} is the Kronecker delta symbol. This measure computes the average existence of edges over all layers of the multiplex network (Lacasa *et al.*, 2015).

Since the proxy record is irregularly sampled, we have first interpolated the data into $N = 2100$ points, leading to the time resolution $\Delta t = t_{i+1} - t_i \approx 5.53$ years $\forall i \in [1, N-1]$. In order to analyse the temporal variation in the environmental dynamics, we applied a sliding-window approach consisting of 100 data points per window. With this choice, each window covers about 547.8 years and is suitable to represent regime changes in the environmental dynamics. MRN is created for each window one by one as the window slides over the time series with 90% overlap.

Principal component analysis

The proxies are representative of processes in the catchment (lithogenics and terrestrial organic matter) or the lacustrine environment (evaporative minerals, aquatic organic matter). To disentangle the different components from the proxies, we have applied PCA to the same set of proxies used in the MRN analysis. Employing the PAST programme (version 4.02) (Hammer *et al.*, 2001) we have used the PCA to decompose the original set of time series to a new set of normalized time series that are

uncorrelated with each other and provide information on the contribution of each proxy to these decomposed time series.

Results and Discussion

The results of MRN analyses are shown in Figure 3. The average overlap ω quantifies the similarities in the dynamics of the components of the multivariate data. Higher ω indicates synchronous or more similar behaviour of proxies. This does not necessarily mean that the values of the components of the data go in the same directions, but that, for example, periodical variations are similar, because one environmental factor acts as the main driving force. Low ω values indicate, in contrast, less synchronous, less similar dynamic behaviour. This can happen, for example, when the system is seriously disturbed (tectonic activity), leading to altered proxy response to forcings, or a change in boundary conditions (e.g. catchment) or a different climate driver.

Lonar Lake

The results of the MRN analysis (Figure 3a) can be broadly divided into two distinct intervals: 8.4–6.2 cal ka (wetter), characterized by more synchronous proxy dynamics (higher ω), and 6.2 cal ka to present (drier), marked by low synchronous proxy dynamics (lower ω). Interestingly, in contrast to the early Holocene wet phase, both intervals of prolonged droughts (PD1 and PD2) shown in Figures 2 and 3 (brown bars) are characterized by low ω values indicating less similar dynamic behaviour. The MRN analysis indicates a sharp regime shift at 6.2 cal ka, coinciding with a known insolation forced shift towards drier conditions. If the criterion of less similar behaviour is associated with drier intervals, then additional drier events can be identified centred at c. 8, 5.9, 5.2, 4.3, 2.7, and 1.4 cal ka. Though not prominently represented in the litholog (Figure 2a), these events have been identified using spectral changes in amino acids pointing to enhanced oxygenation and organic matter degradation, enhanced $\delta^{13}C$ of organic matter, and higher lithogenic matter as indicators of lower lake levels and drier conditions (Menzel *et al.*, 2014).

Tso Moriri Lake

Barring short excursions between 5.8–5.5 and 1.9–1.7 cal ka, low ω values indicating that less similar dynamic behaviour persist from 7 cal ka to present (Figure 3b). Unlike Lonar Lake, lower ω values do not coincide with the onset of drying periods (brown bars in Figure 3b). This denotes that the lacustrine processes represented by the proxies respond to different (multiple) environmental forcings in this lake.

The most notable similarity between the two lakes from different climatic zones is the regime shift at 6.2 cal ka in the central Indian Lonar Lake and at 7 cal ka in the high-altitude Tso Moriri Lake. This discrepancy in timing cannot be attributed to chronological uncertainties as an earlier shift is observed in several other proxy records in the high-altitude Himalaya (Mischke and Zhang, 2010; Kasper *et al.*, 2015; Zhang *et al.*, 2016; Ahlborn *et al.*, 2017). Since there is no evidence for Holocene tectonic activity in the Tso Moriri Lake, we attribute the difference in timing of this extrinsic regime shift to two probable factors: (i) solar insolation forced earlier withdrawal of the ISM and the increasing influence of the westerlies (An *et al.*, 2012; Mishra *et al.*, 2015) in the high-altitude Himalayas; and/or (ii) a change in provenance and catchment contribution which introduced a local forcing that modified the environmental impact preserved in the sediments.

We note that the MRN analysis investigates the variation of the multiple proxy records together. To identify the reasons underlying changes in dynamic behaviour, individual contributions of different proxies to ecosystem change must be determined, and links to climate processes established. The PCA provides decomposition based on a linear model. The association of proxies with specific principal components could represent a certain climate or environmental signal. The mixing matrix (loadings) derived by the PCA can be used to interpret the separate contribution of each proxy to the principal components.

Identifying PC and links to proxies

We have set 50% of the declared variance as the boundary value (corresponding to a loading >0.7) for interpreting the factors.

Lonar Lake

The first five components of the PCA explain 94.44% of the variance in the original data (Table 1) for Lonar Lake. The boundary value constraint (Table 2) confines our interpretation to the first two PCs that together explain 70.35% of the variance in the Lonar proxy data.

PC1 shows positive loadings with carbonate content, $\delta^{13}C_{carb}$ and $\delta^{18}O_{carb}$ (indicators of evaporation), and negative loading for lithogenic content (indicator of lake level) (Table 2). TOC and TN in lake sediments are derived from both terrestrial vegetation brought in by surface runoff and aquatic productivity. All of these proxies are indicators of hydrological changes. We conclude that PC1 is an indicator of I/E (inflow/evaporation)-controlled lake-level changes with positive values during wetter periods. We note the C/N, a productivity indicator, is close to (but does not cross) the 0.7 threshold in PC1 – we attribute this to the organic matter being a combination of terrestrial and aquatic components. PC2 shows high loadings prior to and during periods of strong evaporation (Figures 4e and f), and is therefore considered to be an indicator of salinity changes.

Tso Moriri Lake

The first five components of the PCA explain 98.23% of the variance in the original data (Table 1). However, as with Lonar Lake, the boundary constraint (Table 2) limits us to the first two proxies that explain 78.79% of the variance in this lake. PC1 shows positive loadings with carbonates, $\delta^{13}C_{carb}$ and $\delta^{18}O_{carb}$ (indicators of evaporation), and negative loading for lithogenic content (%) (Table 2). Interestingly, PC1 also shows positive loading for $\delta^{15}N$, which further hints at a change in N sources accompanied by a shift to a more evaporative regime

Table 1. Percentage of total variable variance contained by the individual principal components in the Lonar and Tso Moriri lakes

	Lonar Lake	Tso Moriri Lake
Factors	% variance	% variance
PC1	54.80	53.66
PC2	15.55	25.13
PC3	10.14	11.33
PC4	8.37	6.01
PC5	5.58	2.1

Table 2. Factor loadings for the Lonar and Tso Moriri lakes. Values with declared variance in excess of 50% (i.e. >0.7) are shown in bold

	Lonar Lake		Tso Moriri Lake	
Variable	PC1 (I/E)	PC2 (Salinity)	PC1 (I/E)	PC2 (Terrestrial/aquatic organics)
TOC (%)	**0.88**	−0.16	0.48	**0.85**
$\delta^{13}C_{org}$ (‰)	0.008	**0.82**	0.65	−0.0007
$\delta^{15}N$ (‰)	0.45	**0.70**	**0.90**	0.22
TN (%)	**0.75**	0.03	0.46	**0.77**
C/N	0.57	−0.33	0.23	0.53
Carbonate (%)	**0.89**	0.09	**0.79**	−0.52
Lithogenic (%)	**−0.94**	0.11	**−0.81**	0.49
$\delta^{13}C_{carb}$ (‰)	**0.81**	0.23	**0.95**	−0.03
$\delta^{18}O_{carb}$ (‰)	**0.82**	0.17	**0.93**	−0.27

(increasing $\delta^{18}O$) in the late Holocene (Figure 2b). Hence, we conclude that PC1 is an indicator of I/E-controlled lake-level changes. PC2 shows positive (>0.7) loadings for TOC, TN, with less significance for C/N, and negative for carbonate content. As TOC and TN may be contributed both by terrestrial and aquatic vegetation, the positive (albeit <0.7) loading for C/N implies PC2 to be indicative of the relative contribution of terrestrial versus aquatic organic matter.

Climate forcing of regime shifts in lakes

Meteorological data suggests interannual to decadal-scale ISM variability under the influence of remote forcings induced by SST and/or land surface conditions (Webster *et al.*, 1998; Ummenhofer *et al.*, 2016). ENSO is one of the major forcings that influences the interannual variability of summer monsoon rainfall over India. The time series of year-on-year variations in the summer monsoon rainfall over India for the period AD 1871–2009 indicates that a majority of droughts have occurred during ENSO events, while several wet monsoons have accompanied La Niña episodes (i.e. the cold phase of ENSO) (e.g. Goswami *et al.*, 2006; Ummenhofer *et al.*, 2011; Kurths *et al.*, 2019). Monsoon droughts over India can also arise from interactions between the monsoon convection and the mid-latitude circulation (e.g. Ding and Wang, 2007; Krishnan *et al.*, 2009). Several studies have reported persistent intrusion of cold and dry northwesterly winds from the mid-latitude and subtropical regions of west-central Asia into the Indo-Pakistan region during intense 'monsoon breaks' (e.g. Ramaswamy, 1962; Keshavamurty and Awade, 1974; Raman and Rao, 1981; Kripalani *et al.*, 1997; Joseph and Srinivasan, 1999; Krishnan *et al.*, 2009). This advection of cold and dry northwesterly winds into the monsoon region produces anomalous tropospheric cooling, reduces the meridional temperature gradient, and can weaken the monsoon convective activity in central India while the Himalayan foothills receive enhanced rainfall.

While the long-term ISM variability is linked to solar insolation (Fleitmann *et al.*, 2003; Gupta *et al.*, 2005), the short-term (multidecadal to centennial) fluctuations and extreme events are triggered by a variety of forcings – for example, ENSO, launch of ice rafted debris (IRD) in the north Atlantic (Bond *et al.*, 1997), and the corresponding southward shift of the westerlies (Sinha *et al.*, 2005; Narasimha and Bhattacharyya, 2010; Sun *et al.*, 2016; Srivastava *et al.*, 2017). Regional hydrological patterns resembling ENSO (Prasad *et al.*, 2014) or 'monsoon breaks' (Sinha *et al.*, 2011; Anoop *et al.*, 2013b; Misra *et al.*, 2020) have been identified during the Holocene.

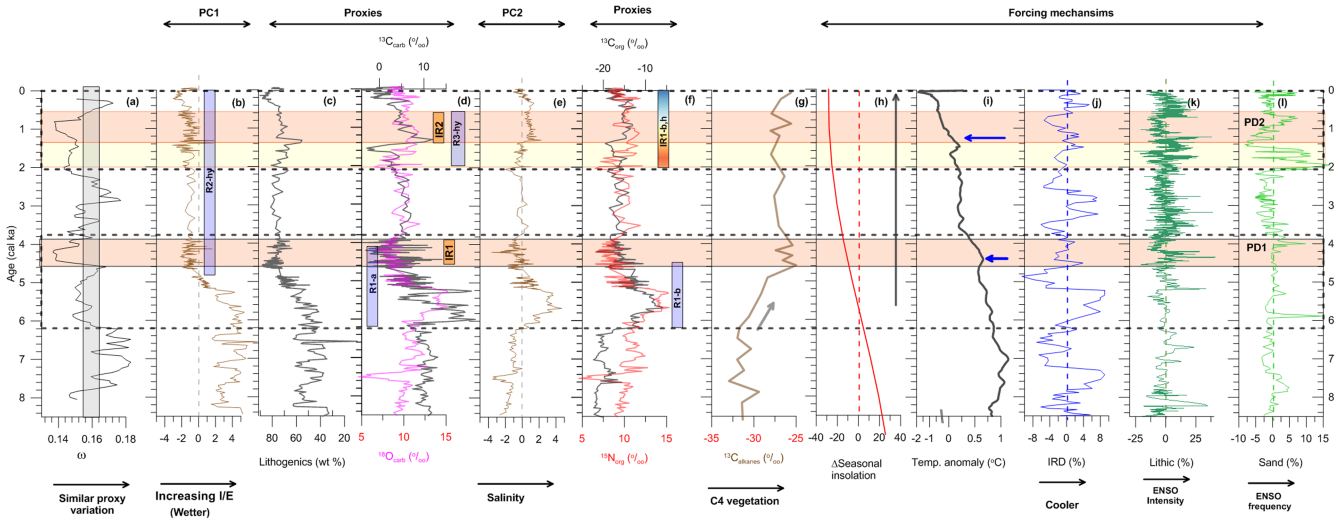

Figure 4. Lonar Lake. (a) Illustration of derived average edge measure calculated in moving windows. The shaded grey area marks the upper 95% confidence interval; (b) PC1, indicative of I/E; (c, d) variation in lithogenic (%) and carbonate isotopes, respectively; (e) PC2 is indicative of salinity changes; (f) isotopic composition of bulk organic matter; (g) isotopic composition of alkanes, indicating shift to C4 vegetation at c. 6.2 cal ka (grey arrow); (h–l) detrended forcing mechanisms (references in text). The dashed grey boxes indicate two intervals when the effect of decreasing seasonal solar insolation [grey arrow in (h)] was amplified by internal forcing mechanisms. R and IR indicate externally and internally forced regime shifts, respectively; suffixes -a, -b, -hy, and -h indicate shifts in atmospheric regimes, biological productivity, hydrology, and human influence. Blue arrows in (i) indicate intensified high-latitude cooling. Coloured bars indicate (independently inferred) prolonged droughts (PD1 and PD2), with darker colours indicating higher intensity. [Colour figure can be viewed at wileyonlinelibrary.com]

To link the proxies to climate change, a clear understanding of proxy sensitivity and their leads and lags within the lacustrine system is essential, as not all proxies uniformly register the impact of climate change (Menzel *et al.*, 2014; Prasad *et al.*, 2016). The decomposed signals derived from the PCA of the Lonar and Tso Moriri cores (Figures 4 and 5) are used to identify temporal variability of sensitive proxies. We have compared the PC scores to the proxies for the following known forcings: solar insolation (Berger and Loutre, 1991), IRD events (Bond *et al.*, 1997), ENSO strength (lithic %, Rein *et al.*, 2005) and frequency of its occurrence (sand %, Conroy *et al.*, 2008), and high-latitude temperature changes (Marcott *et al.*, 2013). It must be noted that these forcings may not operate in isolation. Modelling studies have linked the IRD events to a southward shift of ITCZ along with changes in the trade winds and an asymmetric response of the Hadley circulation (Broccoli *et al.*, 2006). The Atlantic meridional overturning circulation (AMOC) weakening is also associated with a southward movement of the ITCZ and associated changes in precipitation (e.g. Stouffer *et al.*, 2006; McGee *et al.*, 2014). Using grain size data from multiple cores, Thornalley *et al.* (2013) demonstrated that AMOC was weaker during the early and later part of the Holocene, but was strongest between 8 and 6 ka, largely coincident with the early Holocene ISM intensification. However, a detailed comparison for shorter ISM events is presently not possible due to limited time resolution of the Holocene dataset on AMOC changes.

In the following section, we compare PCs with proxies to identify links with climate change, environmental and ecosystem shifts. The PC (proxy) linked with climate change is compared with known ISM forcings to understand mechanisms/pathways triggering climate change and characterize an extrinsic regime shift. We proceed on the premise that any progressive change in the lacustrine system, when independent of forcing mechanisms, and representing an intensification of pre-existing trend is an intrinsic regime shift. Human impact, either in the form of vegetation changes or external nutrient supply, is considered an extrinsic forcing.

In the following, sequential (1, 2, 3) extrinsic (R) and intrinsic regime (IR) shifts are related to changes in atmospheric circulation (a), hydrology (hy), biological productivity (b), and human impact (h).

Lonar Lake

The Lonar Lake PC1 scores show a wetter interval (positive values, Figure 4b) between 8.4 and 6.2 cal ka corresponding to the solar insolation-forced northward migration of the ITCZ (Haug *et al.*, 2001). However, no impact of IRD (Figure 4j) or ENSO events (Figures 4k and l) are evident from PC1 scores (Figure 4b) that show high values and PC2 scores (Figure 4e) that show lower salinities during the wetter early Holocene. The expected gradual ISM weakening during the late Holocene based solely on decreasing solar insolation is not borne out by the Lonar Lake data that is punctuated by two prominent droughts. We propose that the IRD event between 6.2 and 5.2 cal ka (Figure 4j) led to a southward shift of the westerlies causing a reorganization of precipitation pathways/sources and biological productivity as preserved in the isotopic data of carbonates (R1-a, Figure 4d), bulk organic matter (R1-b, Figure 4f), and biomarkers (Figure 4g; Sarkar *et al.*, 2015), respectively. A weaker ISM coupled with intense ENSO events (Figure 4k) results in a decreasing lake level at c. 5.2 cal ka (R2-hy, Figure 4b). Interestingly, the two intervals of prolonged droughts (PD1 between 4.6 and 3.9 cal ka and PD2 between 2 and 0.6 cal ka with intensification between 1.3 and 0.6 cal ka) (Anoop *et al.*, 2013a; Prasad *et al.*, 2014) characterized by the precipitation of evaporite gaylussite in saline waters are not reflected in the PC1 scores, suggesting that their formation was linked to summer evaporation-induced salinity (PC2). A comparison with the forcing mechanisms indicates intensified high-latitude cooling (Marcott *et al.*, 2013) coincident with intense but not very frequent ENSO events (Rein *et al.*, 2005) during PD1. A similar coincidence of frequent, intense ENSO events during high-latitude cooling (Figures 4i, k, and l) is observed during PD2. Interestingly, IRD events centred around 2.7 and 7.5 cal ka (Figure 4j), though causing environmental changes (Figures 3a and 4a), did not trigger droughts in the Lonar Lake. Our results show that during the late Holocene a coincidence of at least two different forcings was needed to amplify their effect on ISM and trigger prolonged droughts.

PC2 scores however, as indicators of salinity, show above-average values only in the two intervals at 6.2–4.6 and 1.3–0.1 cal ka (Figure 4e) with no obvious link to lake-level changes. The former event is characterized by increased

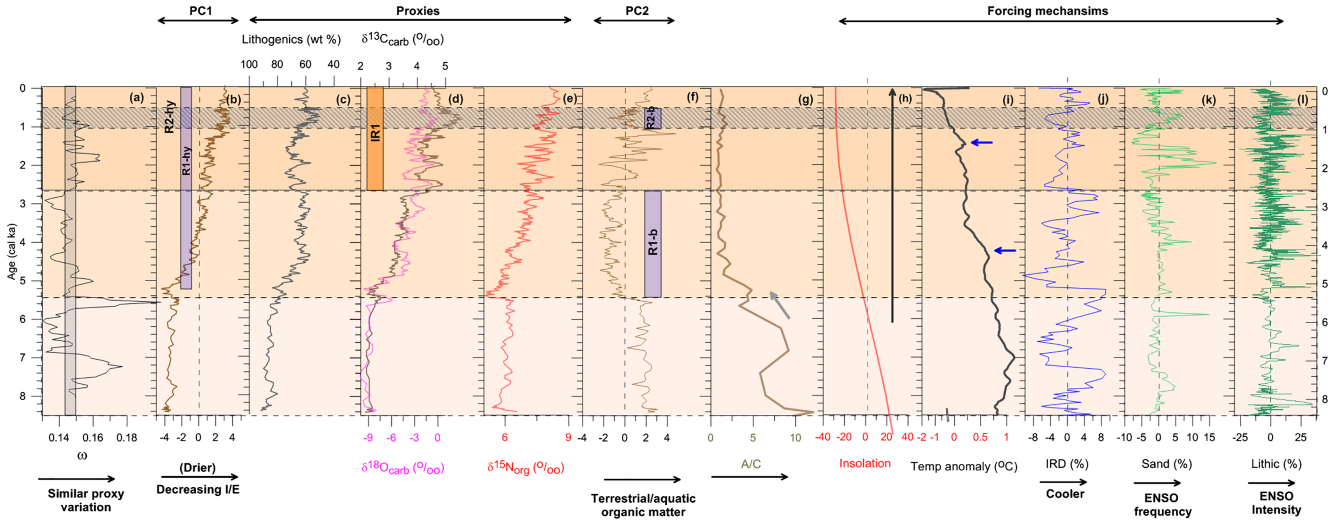

Figure 5. Tso Moriri Lake. (a) Illustration of derived average edge measure calculated in moving windows. The shaded grey area marks the upper 95% confidence interval; (b) PC1, indicative of I/E; (c–e) variation in lithogenic (%), carbonate (%), isotopic composition of carbonates, respectively; (f) PC2 is indicative of terrestrial vs aquatic organic matter; (g) A/C represents *Artemisia/Chenopodiaceae*, grey arrow marks a shift to lower values; (h–l) detrended forcing mechanisms (references in text). R and IR indicate externally and internally forced regime shifts, respectively; suffixes -hy and -b indicate shifts in hydrology and terrestrial/aquatic organic matter content. Blue arrows in (i) indicate intensified high-latitude cooling. Yellow and orange boxes indicate (independently inferred) drier intervals with darker colours indicating intensity. [Colour figure can be viewed at wileyonlinelibrary.com]

biological productivity in a saline lake (Figure 4f). The second interval is additionally accompanied by increasing human influence in the Lonar catchment c. 1.2 cal ka (Mishra *et al.*, 2018b).

We can identify three limnological regime shifts in the Lonar proxy data. The first extrinsic regime shift that began at 6.2 cal ka was triggered by decreased solar insolation and increased IRD in the north Atlantic, and had a twofold impact: (i) a change in precipitation pathways (6.2–4.6 cal ka, R1-a) and lake-level lowering at 5.2 cal ka (R2-hy) culminating in PD1 (4.6–3.9 cal ka, IR1). It is albeit likely that PD1 was an intrinsic regime shift representing a nonlinear response to previously accumulated primary climate forcings (cooler high latitudes and IRD event), as a similar coincidence of climate forcings during the early Holocene (7–6.2 cal ka, Figures 4i and j) did not result in a prolonged drought; and (ii) resulted in an increased biological productivity in a saline lake (6.2–4.6 cal ka, R1-b). The catchment also showed a shift from C3 to C4-type terrestrial vegetation at 6.2 cal ka (Figure 4g), confirming a shift to drier climate in response to R1-a.

The second extrinsic regime shift began at c. 2 cal ka (R3-hy, increase in salinity, Figure 4b) during drier climate triggered by frequent and intense ENSO events (Figures 4k and l) during an interval of high-latitude cooling (Figure 4i). However, it is difficult to conclude whether the intensification of drier conditions in PD2 (1.4–0.6 cal ka, IR2) is a response to threshold changes or to persistent ENSO (Figure 4l). An overlapping third regime shift marked by increasing biological productivity in the Lonar Lake extends from 1.2 to present (IR-b, h, Figure 4f) when increasing human influence is observed in pollen and nitrogen isotope data from 1.2 cal ka (Mishra *et al.*, 2018b).

Tso Moriri Lake

An expected trend of insolation-forced hydrological changes (R1-hy, Figure 5b) is observed with an increase in carbonate precipitation c. 5.5 cal ka (Figure 2). The decrease in I/E at 5.2 cal ka lags behind the solar forcing at c. 6.2 cal ka (Figure 5h). The coincidence of $\delta^{18}O$ with $\delta^{15}N$ (Figures 5d and e) from 5.5 cal ka suggests a change in dominant inflow to the northern source, indicating that the MRN shift at 7 cal ka (Figure 3b) is likely a result of climate change (increasing westerly influence) rather than a provenance change. A concomitant decrease in vegetation *Artemisia/Chenopodiaceae* (A/C, an indicator of precipitation/evaporation; Leipe *et al.*, 2014) confirms the trend towards drier climate. Intensified drying, characterized by aragonite precipitation, is seen from 2.7 cal ka to present (Mishra *et al.*, 2015). Barring a short interval 1.2–0.6 cal ka, marked by decreased inflow (R2-hy, Figure 5b) and higher evaporation that coincides with frequent ENSO events, the Tso Moriri palaeorecord was primarily dominated by insolation and does not show any impact of ENSO or IRD events. The shift to drier conditions at 2.7 cal ka appears to be a response to progressive decrease in I/E that began at 5.2 cal ka. PC2, an indicator of terrestrial versus aquatic organic matter (Figure 5f), has lowest scores from 5.4 to 2.7 cal ka (R1-b) and 1.2 to 0.6 cal ka (R2-b) due to decreased influx of terrestrial organic matter from reduced inflow.

Regional differences in proxy response to climate forcing

Based on the proxy data it appears that terrestrial vegetation shows the earliest (c. 6.2 cal ka), though gradual, response to insolation forcing in both climate regions. In Lonar catchment, we observe the beginning of change from C3 to C4 grass in pollen of moist deciduous forest that was still present (Prasad *et al.*, 2014; Sarkar *et al.*, 2015). Similarly, the Tso Moriri pollen record shows decreasing A/C around 6 cal ka. However, the hydrochemical and productivity responses differ in both regions. Firstly, salinity and productivity changes in the Lonar Lake are concurrent with vegetation shifts, followed by a drop in lake level at 5.2 cal ka. However, in the Tso Moriri Lake, the fall in lake level and increase in salinity at c. 5.5 cal ka lag behind vegetation changes. Secondly, the productivity signal in Tso Moriri is related to changing terrestrial organic input rather than lacustrine productivity shifts. We attribute the inter-regional hydrological differences to the large size of the Tso Moriri Lake and multiple inflow sources that resulted in the 'damping' of the climate forcing. In addition to the insolation-induced shift at 6.2 cal ka, the only other common event in both the lakes is reduced I/E between c. 1.3 and 0.6 cal ka, coincident with frequent, intense ENSO and high-latitude cooling.

In the Tso Moriri Lake, the proxy data indicate two extrinsic limnologic regime shifts, the first beginning c. 5.5 cal ka (R1-hy, Figure 5b) was a response to insolation-forced decreasing I/E, while the second occurring between 1.2 and 0.6 cal ka (R2-hy) coincides with frequent ENSO conditions (Figure 5k). Both shifts were accompanied by a decrease in terrestrial organic matter influx (Figure 5f, R1-b, R2-b) but without major change in the terrestrial vegetation cover. The intensification of the drying trend beginning 2.7 cal ka, without an apparent additional forcing (ENSO or IRD), represents an intrinsic regime shift (IR1-hy) as the threshold for precipitation of aragonite is reached. The apparent insensitivity to climate-forced regime shifts in the Tso Moriri proxy data could probably be related to the large lake size and its location in a cold desert, meaning that lake level is inflow (snowmelt) dominated, and any small change in precipitation would not have a significant impact on its hydrology.

Summary and Outlook

Our investigation into the efficacy of data analyses techniques in extracting the inherent proxy response to climate forcings and environmental change, and in detecting regime shifts, provides useful insights into their potential and limitations. We have used MRN, which considers all proxy data together, to investigate critical regime transitions occurring synchronously in multivariate time series from two lakes located in different climate regions. This method, which identifies entrapped critical climate transitions in proxy data, successfully identified climate shifts in the ISM-dominated Lonar Lake. Synchronous dynamics in all proxies (higher values of ω) are associated with strong climate forcings, felt by all lacustrine ecosystem processes, and less similar dynamical behaviour of the proxies (low values of ω) are associated with drier periods. However, in the Tso Moriri Lake we have not been able to find extended synchronous dynamics in all proxies, in particular during drier periods (no association of ω with drier periods). This indicates equal impact of several concurrent external forcings. The hydrology of this lake is governed by the ISM, westerlies, and meltwater inflow. A change in any of these sources will result in a modified environmental forcing and an altered proxy–climate relationship. Therefore, the MRN-based similarity indicator ω can be interpreted as an indicator of a single environmental forcing.

The results of a PCA provided insights into the role of individual proxies, enabled comparison with forcings to document the progressive impact of climate change, and distinguished between extrinsic and intrinsic regime shifts.

Our results show that regime shifts caused by climate forcings are more common during the late Holocene in central India due to the disproportionately large impact of any small change in precipitation during drying intervals. In contrast, larger lakes located in cold deserts on the fringes of the ITCZ appear to be relatively immune to climate forcings. Clearly, there are regional differences in the impact of climate forcings based on archive location and sensitivity. This also places limitations on the potential of data analysis techniques in identifying overarching climate forcing mechanisms.

As the proxies are measured on samples from the same depth (age), it is possible to discuss leads and lags in the ecosystem. The biosphere is most sensitive to climate forcings with changes in terrestrial vegetation, followed by hydrochemical changes. Therefore, a potential role of vegetation–atmosphere feedback will need to be considered in triggering droughts in central India in future modelling studies. In contrast to central India, there is no dramatic change in the Tso Moriri catchment vegetation, excluding a significant influence of vegetation on the local climate.

We acknowledge that due to data and chronology limitations our study could not adequately focus on other factors affecting the ISM (e.g. changes in the position of the Indo Pacific Warm Pool, changes in Eurasian snow cover, or vegetation–climate feedback mechanisms – particularly in central India). However, our investigations can provide a conceptual model to explain links between forcings and regional climate change that can be tested in climate models to provide an improved understanding of the ISM dynamics and their impact on ecosystems.

Acknowledgements—This study received funding from DFG projects MA4759/8 (IUCLiD) and MA4759/11 as well as from the European Union's Horizon 2020 research and innovation programme to the TiPES project (Grant Agreement No. 820970 to NM and BG), TUBITAK Grant No. 118C236 and the internal research support program (BAF) of Kadir Has University (DE), and the DST-INSPIRE (DST/INSPIRE/04/2015/002769) faculty program (PM). The lakes data (Lonar and Tso Moriri) used in this study was generated in the German Research Foundation (FOR 1380) funded HIMPAC (Himalayas: Modern and Past Climates, PR 755/7–2) project. This is TiPES contribution #33.

Conflict of Interest

The authors declare no conflict of interest.

Data Availability Statement

Data is available upon request.

References

Ahlborn M, Haberzettl T, Wang J, Henkel K, Kasper T, Daut G, Zhu L, Mäusbacher R. 2017. Synchronous pattern of moisture availability on the southern Tibetan Plateau since 17.5 cal. ka BP – the Tangra Yumco lake sediment record. *Boreas* **46**: 229–241. https://doi.org/10.1111/bor.12204

An Z, Colman SM, Zhou W, Li X, Brown ET, Jull AT, Cai Y, Huang Y, Lu X, Chang H, Song Y. 2012. Interplay between the westerlies and Asian monsoon recorded in Lake Qinghai sediments since 32 ka. *Scientific Reports* **2**: 619–626. https://doi.org/10.1038/srep00619

Anoop A, Prasad S, Plessen B, Basavaiah N, Gaye B, Naumann R, Menzel P, Weise S, Brauer A. 2013a. Palaeoenvironmental implications of evaporative gaylussite crystals from Lonar Lake, central India. *Journal of Quaternary Science* **28**: 349–359. https://doi.org/10.1002/jqs.2625

Anoop A, Prasad S, Krishnan R, Naumann R, Dulski P. 2013b. Intensified monsoon and spatiotemporal changes in precipitation patterns in the NW Himalaya during the early-mid Holocene. *Quaternary International* **313–314**: 74–84. https://doi.org/10.1016/j.quaint.2013.08.014

Basavaiah N, Wiesner MG, Anoop A, Menzel P, Nowaczyk NR, Deenadayalan K, Brauer A, Gaye B, Naumann R, Riedel N, Prasad MS. 2014. Physicochemical analyses of surface sediments from the Lonar Lake, central India – implications for palaeoenvironmental reconstruction. *Fundamental and Applied Limnology/Archiv für Hydrobiologie* **184**: 51–68. https://doi.org/10.1127/1863-9135/2014/0515

Berger A, Loutre MF. 1991. Insolation values for the climate of the last 10 million years. *Quaternary Science Reviews* **10**: 297–317. https://doi.org/10.1016/0277-3791(91)90033-Q

Bhushan R, Sati SP, Rana N, Shukla AD, Mazumdar AS, Juyal N. 2018. High-resolution millennial and centennial scale Holocene monsoon variability in the Higher Central Himalayas. *Palaeogeography, Palaeoclimatology, Palaeoecology* **489**: 95–104. https://doi.org/10.1016/j.palaeo.2017.09.032

Bird BW, Polisar PJ, Lei Y, Thompson LG, Yao T, Finney BP, Bain DJ, Pompeani DP, Steinman BA. 2014. A Tibetan lake sediment record of Holocene Indian summer monsoon variability. *Earth and Planetary Science Letters* **399**: 92–102. https://doi.org/10.1016/j.epsl.2014.05.017

Birks HH, Birks HJB. 2006. Multi-proxy studies in palaeolimnology. *Vegetation History and Archaeobotany* **15**: 235–251. https://doi.org/10.1007/s00334-006-0066-6

Bond G, Showers W, Cheseby M, Lotti R, Almasi P, DeMenocal P, Priore P, Cullen H, Hajdas I, Bonani G. 1997. A pervasive millennial-scale cycle in North Atlantic Holocene and glacial climates. *Science* **278**: 1257–1266. https://doi.org/10.1126/science.278.5341.1257

Broccoli AJ, Dahl KA, Stouffer RJ. 2006. Response of the ITCZ to Northern Hemisphere cooling. *Geophysical Research Letters* **33**(1). https://doi.org/10.1029/2005GL024546

Chen F, Chen J, Huang W, Chen S, Huang X, Jin L, Jia J, Zhang X, An C, Zhang J, Zhao Y. 2019. Westerlies Asia and monsoonal Asia: spatiotemporal differences in climate change and possible mechanisms on decadal to sub-orbital timescales. *Earth-Science Reviews* **192**: 337–354. https://doi.org/10.1016/j.earscirev.2019.03.005

Conroy JL, Overpeck JT, Cole JE, Shanahan TM, Steinitz-Kannan M. 2008. Holocene changes in eastern tropical Pacific climate inferred from a Galápagos lake sediment record. *Quaternary Science Reviews* **27**: 1166–1180. https://doi.org/10.1016/j.quascirev.2008.02.015

Ding Q, Wang B. 2007. Intraseasonal teleconnection between the summer Eurasian wave train and the Indian monsoon. *Journal of Climate* **20**: 3751–3767. https://doi.org/10.1175/JCLI4221.1

Dixit Y, Hodell DA, Petrie CA. 2014a. Abrupt weakening of the summer monsoon in northwest India ~4100 yr ago. *Geology* **42**: 339–342. https://doi.org/10.1130/G35236.1

Dixit Y, Hodell DA, Sinha R, Petrie CA. 2014b. Abrupt weakening of the Indian summer monsoon at 8.2 kyr B.P. *Earth and Planetary Science Letters* **391**: 16–23. https://doi.org/10.1016/j.epsl.2014.01.026

Eroglu D, McRobie FH, Ozken I, Stemler T, Wyrwoll KH, Breitenbach SF, Marwan N, Kurths J. 2016. See saw relationship of the Holocene East Asian–Australian summer monsoon. *Nature Communications* **7**: 1–7.

Eroglu D, Marwan N, Stebich M, Kurths J. 2018. Multiplex recurrence networks. *Physical Review E* **97**: 1–9, 012312. https://doi.org/10.1103/PhysRevE.97.012312

Fleitmann D, Burns SJ, Mudelsee M, Neff U, Kramers J, Mangini A, Matter A. 2003. Holocene forcing of the Indian monsoon recorded in a stalagmite from Southern Oman. *Science* **300**: 1737–1740.

Folke C, Carpenter S, Walker B, Scheffer M, Elmqvist T, Gunderson L, Holling CS. 2004. Regime shifts, resilience, and biodiversity in ecosystem management. *Annual Review of Ecology, Evolution, and Systematics* **35**: 557–581.

Gadgil S. 2003. The Indian monsoon and its variability. *Annual Review of Earth and Planetary Sciences* **31**: 429–467. https://doi.org/10.1146/annurev.earth.31.100901.141251

Gadgil S. 2004. Extremes of the Indian summer monsoon rainfall, ENSO and equatorial Indian Ocean oscillation. *Geophysical Research Letters* **31**(12), L12213. https://doi.org/10.1029/2004GL019733

Goswami BN, Venugopal V, Sengupta D, Madhusoodanan MS, Xavier PK. 2006. Increasing trend of extreme rain events over India in a warming environment. *Science* **314**: 1442–1445. https://doi.org/10.1126/science.1132027

Goswami BN, Boers N, Rheinwalt A, Marwan N, Heitzig J, Breitenbach SF, Kurths J. 2018. Abrupt transition in time series with uncertainties. *Nature Communications* **9**: 1–10.

Gupta AK, Das M, Anderson DM. 2005. Solar influence on the Indian summer monsoon during the Holocene. *Geophysical Research Letters*, **32**(17). https://doi.org/10.1029/2005GL022685

Hammer Ø, Harper DAT, Ryan PD. 2001. PAST: paleontological statistics software package for education and data analysis. *Palaeontologia Electronica* **4**: 1–9.

Haug GH, Hughen KA, Sigman DM, Peterson LC, Röhl U. 2001. Southward migration of the intertropical convergence zone through the Holocene. *Science* **293**: 1304–1308. https://doi.org/10.1126/science.1059725

Hodell DA, Schelske CL. 1998. Production, sedimentation, and isotopic composition of organic matter in Lake Ontario. *Limnology and Oceanography* **43**: 200–214.

Jhingran AG, Rao KV. 1958. Lonar Lake and its salinity. *Records of the Geological Survey of India* **85**: 313–334.

Joseph PV, Srinivasan J. 1999. Rossby waves in May and the Indian summer monsoon rainfall. *Tellus A* **51**: 854–864.

Joshi AA, Kanekar PP, Kelkar AS, Shouche YS, Vani AA, Borgave SB, Sarnaik SS. 2008. Cultivable bacterial diversity of alkaline Lonar Lake, India. *Microbial Ecology* **55**: 163–172. https://doi.org/10.1007/s00248-007-9264-8

Jourdan F, Moynier F, Koeberl C, Eroglu S. 2011. $^{40}Ar/^{39}Ar$ age of the Lonar crater and consequence for the geochronology of planetary impacts. *Geology* **39**: 671–674.

Kasper T, Haberzettl T, Wang J, Daut G, Doberschütz S, Zhu L, Mäusbacher R. 2015. Hydrological variations on the Central Tibetan Plateau since the Last Glacial Maximum and their teleconnection to inter-regional and hemispheric climate variations. *Journal of Quaternary Science* **30**: 70–78. https://doi.org/10.1002/jqs.2759

Keshavamurty RN, Awade ST. 1974. *Energy Conversions During Weak Monsoon*. Indian Institute of Tropical Meteorology: Pune.

Kripalani RH, Kulkarni A, Singh SV. 1997. Association of the Indian summer monsoon with the Northern Hemisphere mid-latitude circulation. *International Journal of Climatology* **17**: 1055–1067.

Krishnan R, Kumar V, Sugi M, Yoshimura J. 2009. Internal feedbacks from monsoon–midlatitude interactions during droughts in the Indian summer monsoon. *Journal of the Atmospheric Sciences* **66**: 553–578. https://doi.org/10.1175/2008JAS2723.1

Kumar KK, Rajagopalan B, Cane MA. 1999. On the weakening relationship between the Indian monsoon and ENSO. *Science* **284** (5423): 2156–2159.

Kurths J, Agarwal A, Shukla R, Marwan N, Rathinasamy M, Caesar L, Krishnan R, Merz M. 2019. Unravelling the spatial diversity of Indian precipitation teleconnections via a non-linear multi-scale approach. *Nonlinear Processes in Geophysics* **26**: 251–266.

Lacasa L, Nicosia V, Latora V. 2015. Network structure of multivariate time series. *Scientific Reports* **5**: 1–9, 15508. https://doi.org/10.1038/srep15508

Lechleitner FA, Breitenbach FM, Cheng H, Plessen B, Rehfeld K, Goswami B, Marwan N, Eroglu D, Adkins J, Haug G. 2017. Climatic and in-cave influences on $\delta^{18}O$ and $\delta^{13}C$ in a stalagmite from northeastern India through the last deglaciation. *Quaternary Research* **88**: 458–471.

Leipe C, Demske D, Tarasov PE, HIMPAC Project Members. 2014. A Holocene pollen record from the northwestern Himalayan lake Tso Moriri: implications for palaeoclimatic and archaeological research. *Quaternary International* **348**: 93–112.

Lotter AF. 2003. Multi-proxy climatic reconstructions. *Global Change in the Holocene* 373–383.

Marcott SA, Shakun JD, Clark PU, Mix AC. 2013. A reconstruction of regional and global temperature for the past 11,300 years. *Science* **339**(6124): 1198–1201.

Marwan N, Donges JF, Zou Y, Donner RV, Kurths J. 2009. Complex network approach for recurrence analysis of time series. *Physics Letters A* **373**: 4246–4254.

McGee D, Donohoe A, Marshall J, Ferreira D. 2014. Changes in ITCZ location and cross-equatorial heat transport at the Last Glacial Maximum, Heinrich Stadial 1, and the mid-Holocene. *Earth and Planetary Science Letters* **390**: 69–79.

Menzel P, Gaye B, Wiesner MG, Prasad S, Stebich M, Das BK, Anoop A, Riedel N, Basavaiah N. 2013. Influence of bottom water anoxia on nitrogen isotopic ratios and amino acid contributions of recent sediments from small eutrophic Lonar Lake, central India. *Limnology and Oceanography* **58**: 1061–1074. https://doi.org/10.4319/lo.2013.58.3.1061

Menzel P, Gaye B, Mishra PK, Anoop A, Basavaiah N, Marwan N, Plessen B, Prasad S, Riedel N, Stebich M, Wiesner MG. 2014. Linking Holocene drying trends from Lonar Lake in monsoonal central India to North Atlantic cooling events. *Palaeogeography, Palaeoclimatology, Palaeoecology* **410**: 164–178.

Meyers PA. 1997. Organic geochemical proxies of paleoceanographic, paleolimnologic, and paleoclimatic processes. *Organic Geochemistry* **27**: 213–250. https://doi.org/10.1016/S0146-6380(97)00049-1

Meyers PA, Ishiwatari R. 1993. Lacustrine organic geochemistry – an overview of indicators of organic matter sources and diagenesis in lake sediments. *Organic Geochemistry* **20**: 867–900. https://doi.org/10.1016/0146-6380(93)90100-P

Mischke S, Zhang C. 2010. Holocene cold events on the Tibetan Plateau. *Global and Planetary Change* **72**: 155–163. https://doi.org/10.1016/j.gloplacha.2010.02.001

Mishra C, Humbert-Droz B. 1998. Avifaunal survey of Tsomoriri Lake and adjoining Nuro Sumdo Wetland in Ladakh, Indian trans-Himalaya. *Forktail* **14**: 67–69.

Mishra PK, Anoop A, Jehangir A, Prasad S, Menzel P, Schettler G, Naumann R, Weise S, Andersen N, Yousuf AR, Gaye B. 2014. Limnology and modern sedimentation patterns in high altitude Tso Moriri Lake, NW Himalaya – implications for proxy development. *Fundamental and Applied Limnology/Archiv für Hydrobiologie* **185**: 329–348. https://doi.org/10.1127/fal/2014/0664

Mishra PK, Anoop A, Schettler G, Prasad S, Jehangir A, Menzel P, Naumann R, Yousuf AR, Basavaiah N, Deenadayalan K, Wiesner MG. 2015. Reconstructed late Quaternary hydrological changes from Lake Tso Moriri, NW Himalaya. *Quaternary International* **371**: 76–86. https://doi.org/10.1016/j.quaint.2014.11.040

Mishra PK, Prasad S, Jehangir A, Anoop A, Yousuf AR, Gaye B. 2018a. Investigating the role of meltwater versus precipitation seasonality in abrupt lake-level rise in the high-altitude Tso Moriri Lake (India). *Palaeogeography, Palaeoclimatology, Palaeoecology* **493**: 20–29. https://doi.org/10.1016/j.palaeo.2017.12.026

Mishra PK, Prasad S, Marwan N, Anoop A, Krishnan R, Gaye B, Basavaiah N, Stebich M, Menzel P, Riedel N. 2018b. Contrasting pattern of hydrological changes during the past two millennia from central and northern India: regional climate difference or anthropogenic impact? *Global and Planetary Change* **161**: 97–107. https://doi.org/10.1016/j.gloplacha.2017.12.005

Misra S, Bhattacharya S, Mishra PK, Misra KG, Agrawal S, Anoop A. 2020. Vegetational responses to monsoon variability during Late Holocene: inferences based on carbon isotope and pollen record from the sedimentary sequence in Dzukou Valley, NE India. *Catena* **194**: 1–11.

Narasimha R, Bhattacharyya S. 2010. A wavelet cross-spectral analysis of solar–ENSO–rainfall connections in the Indian monsoons. *Applied and Computational Harmonic Analysis* **28**: 285–295.

Prasad S, Kusumgar S, Gupta SK. 1997. A mid to late Holocene record of palaeoclimatic changes from Nal Sarovar: a palaeodesert margin lake in western India. *Journal of Quaternary Science* **12**(2): 153–159.

Prasad S, Anoop A, Riedel N, Sarkar S, Menzel P, Basavaiah N, Krishnan R, Fuller D, Plesse B, Gaye B, Röhl U, Wilkes H, Sachse D, Sawant R, Wiesner MG, Stebich M. 2014. Prolonged monsoon droughts and links to Indo-Pacific warm pool: a Holocene record from Lonar Lake, central India. *Earth and Planetary Science Letters* **391**: 171–182. https://doi.org/10.1016/j.epsl.2014.01.043

Prasad S, Mishra PK, Menzel P, Gaye B, Jehangir A, Yousuf AR. 2016. Testing the validity of productivity proxy indicators in high altitude Tso Moriri Lake, NW Himalaya (India). *Palaeogeography, Palaeoclimatology, Palaeoecology* **449**: 421–430.

Prasanna V. 2014. Impact of monsoon rainfall on the total foodgrain yield over India. *Journal of Earth System Science* **123**: 1129–1145. https://doi.org/10.1007/s12040-014-0444-x

Raj R, Chamyal LS, Prasad V, Sharma A, Tripathi JK, Verma P. 2015. Holocene climatic fluctuations in the Gujarat Alluvial Plains based on a multiproxy study of the Pariyaj Lake archive, western India. *Palaeogeography, Palaeoclimatology, Palaeoecology* **421**: 60–74.

Raman CRV, Rao YP. 1981. Blocking highs over Asia and monsoon droughts over India. *Nature* **289**: 271–273.

Ramaswamy C. 1962. Breaks in the Indian summer monsoon as a phenomenon of interaction between the easterly and the sub-tropical westerly jet streams. *Tellus* **3**: 337–349.

Ramsey CB. 2008. Deposition models for chronological records. *Quaternary Science Reviews* **27**: 42–60.

Ramsey CB. 2009. Bayesian analysis of radiocarbon dates. *Radiocarbon* **51**: 337–360.

Rehfeld K, Marwan N, Heitzig J, Kurths J. 2011. Comparison of correlation analysis techniques for irregularly sampled time series. *Nonlinear Processes in Geophysics* **18**(3): 389–404.

Reimer PJ, Baillie MGL, Bard E, Bayliss A, Beck JW, Blackwell PG, Ramsey CB, Buck CE, Burr GS, Edwards RL. 2009. IntCal09 and Marine09 radiocarbon age calibration curves, 0–50,000 years cal BP. *Radiocarbon* **51**: 1111–1150.

Rein B, Lu A, Reinhardt L, Sirocko F, Wolf A, Dullo W, Nin E. 2005. El Niño variability off Peru during the last 20,000 years. *Paleoceanography* **20**: 1–18. https://doi.org/10.1029/2004PA001099

Riedel N, Stebich M, Anoop A, Basavaiah N, Menzel P, Prasad S, Sachse D, Sarkar S, Wiesner M. 2015. Modern pollen vegetation relationships in a dry deciduous monsoon forest: a case study from Lonar Crater Lake, central India. *Quaternary International* **371**: 268–279. https://doi.org/10.1016/j.quaint.2015.01.046

Sahai AK, Grimm AM, Satyan V, Pant GB. 2003. Long-lead prediction of Indian summer monsoon rainfall from global SST evolution. *Climate Dynamics* **20**: 855–863. https://doi.org/10.1007/s00382-003-0306-8

Sarkar S, Prasad S, Wilkes H, Riedel N, Stebich M, Basavaiah N, Sachse D. 2015. Monsoon source shifts during the drying mid-Holocene: biomarker isotope based evidence from the core "monsoon zone" (CMZ) of India. *Quaternary Science Reviews* **123**: 144–157. https://doi.org/10.1016/j.quascirev.2015.06.020

Scheffer M, Carpenter S, Foley SF, Folke C, Walker B. 2001. Catastrophic shifts in ecosystems. *Nature* **413**: 591–596.

Sengupta S, Sarkar A. 2006. Stable isotope evidence of dual (Arabian Sea and Bay of Bengal) vapour sources in monsoonal precipitation over north India. *Earth and Planetary Science Letters* **250**: 511–521. https://doi.org/10.1016/j.epsl.2006.08.011

Shashikanth K, Ghosh S, Karmakar VHS. 2018. Future projections of Indian summer monsoon rainfall extremes over India with statistical downscaling and its consistency with observed characteristics. *Climate Dynamics* **51**: 1–15. https://doi.org/10.1007/s00382-017-3604-2

Sinha A, Cannariato KG, Stott LD, Li H-C, You C-F, Cheng H, Edwards RL, Singh IB. 2005. Variability of Southwest Indian summer monsoon precipitation during the Bølling-Ållerød. *Geology* **33**: 813–816. https://doi.org/10.1130/G21498.1

Sinha A, Stott L, Berkelhammer M, Cheng H, Edwards RL, Buckley B, Aldenderfer M, Mudelsee M. 2011. A global context for megadroughts in monsoon Asia during the past millennium. *Quaternary Science Reviews* **30**: 47–62. https://doi.org/10.1016/j.quascirev.2010.10.005

Srivastava P, Agnihotri R, Sharma D, Meena N, Sundriyal YP, Saxena A, Bhushan R, Sawlani R, Banerji US, Sharma C, Bisht P. 2017. 8000-year monsoonal record from Himalaya revealing reinforcement of tropical and global climate systems since mid-Holocene. *Scientific Reports* **7**: 1–10. https://doi.org/10.1038/s41598-017-15143-9

Stouffer RJ, Yin J, Gregory JM, Dixon KW, Spelman MJ, Hurlin W, Weaver AJ, Eby M, Flato GM, Hasumi H. 2006. Investigating the causes of the response of the thermohaline circulation to past and future climate changes. *Journal of Climate* **19**: 1365–1387.

Stuiver M. 1975. Climate versus changes in ^{13}C content of the organic component of lake sediments during the Late Quarternary. *Quaternary Research* **5**: 251–262.

Sun Q, Shan Y, Sein K, Su Y, Zhu Q, Wang L, Sun J, Gu Z, Chu G. 2016. A 530 year long record of the Indian Summer Monsoon from carbonate varves in Maar Lake Twintaung, Myanmar. *Journal of Geophysical Research: Atmospheres* **121**: 5620–5630.

Swart PK. 1983. Carbon and oxygen isotope fractionation in scleractinian corals: a review. *Earth-Science Reviews* **19**: 51–80.

Talbot MR, Lærdal T. 2000. The Late Pleistocene–Holocene palaeolimnology of Lake Victoria, East Africa, based upon elemental and isotopic analyses of sedimentary organic matter. *Journal of Paleolimnology* **23**: 141–164.

Thomas ZA. 2016. Using natural archives to detect climate and environmental tipping points in the earth system. *Quaternary Science Reviews* **152**: 60–71. https://doi.org/10.1016/j.quascirev.2016.09.026

Thornalley DJR, Blaschek M, Davies FJ, Praetorius S, Oppo DW, McManus JF, Hall IR, Kleiven H, Renssen H, McCave IN. 2013. Long-term variations in Iceland–Scotland overflow strength during the Holocene. *Climate of the Past* **9**: 2073–2084.

Ummenhofer CC, Gupta AS, Li Y, Taschetto AS, England MH. 2016. Multi-decadal modulation of the El Nino–Indian monsoon relationship by Indian Ocean variability. *Environmental Research Letters* **6**: 1–8. https://doi.org/10.1088/1748-9326/6/3/034006

Wang B, Liu J, Kim H, Webster PJ, Yim S, Xiang B. 2013. Northern Hemisphere summer monsoon intensified by mega-El Niño/southern oscillation and Atlantic multidecadal oscillation. *PNAS* **110**: 5347–5352. https://doi.org/10.1073/pnas.1219405110

Webster PJ, Magana VO, Palmer TN, Shukla J, Tomas RA, Yanai M, Yasunari T. 1998. Monsoons: processes, predictability, and the prospects for prediction. *Journal of Geophysical Research: Oceans* **103**: 14451–14510.

Williams JW, Blois JL, Shuman BN. 2011. Extrinsic and intrinsic forcing of abrupt ecological change: case studies from the late Quaternary. *Journal of Ecology* **99**(3): 664–677.

Xu H, Ai L, Tan L, An Z. 2006. Stable isotopes in bulk carbonates and organic matter in recent sediments of Lake Qinghai and their climatic implications. *Chemical Geology* **235**: 262–275. https://doi.org/10.1016/j.chemgeo.2006.07.005

Zhang E, Yongbo W, Weiwei S, Ji S. 2016. Holocene Asian monsoon evolution revealed by a pollen record from an alpine lake on the southeastern margin of the Qinghai-Tibetan Plateau, China. *Climate of the Past* **12**: 415–427.